Coulomb blockade of Cooper pair tunneling and parity effects in the Cooper pair transistor

S. Corlevi,[1] W. Guichard,[1,2] F. W. J. Hekking,[2] and D. B. Haviland[1]
[1]*Nanostructure Physics, Royal Institute of Technology, 10691 Stockholm, Sweden*
[2]*University Joseph Fourier and CNRS, Boîte Postale 166, 25 Avenue des Martyrs, 38042 Grenoble-Cedex 09, France*
(Received 9 June 2006; revised manuscript received 5 October 2006; published 13 December 2006)

We have measured the Cooper pair transistor (CPT) in a tunable electromagnetic environment consisting of four one-dimensional superconducting quantum interference device arrays. The transport properties of the CPT in the high impedance limit, $Z_{\mathrm{env}} \gg R_Q \simeq 6.45\ \mathrm{k}\Omega$, are studied for different ratios of the Josephson coupling energy to the charging energy. As the impedance of the environment is increased, the current-voltage characteristic (IVC) of the CPT develops a Coulomb blockade of Cooper pair tunneling and the measured IVCs agree qualitatively with a theory based on quasicharge dynamics for a CPT. Increasing the impedance of the environment induces a transition in the modulation of the IVC with the gate charge from e-periodic to $2e$-periodic.

DOI: 10.1103/PhysRevB.74.224505 PACS number(s): 74.50.+r, 73.23.Hk, 73.40.Gk

I. INTRODUCTION

The interplay between charge quantization and superconductivity offers the possibility to study macroscopic quantum phenomena in small-capacitance Josephson junction circuits. One of the most extensively studied devices in this context is the Cooper pair transistor (CPT), which consists of two Josephson junctions in series, with a gate capacitively coupled to the small island formed between the two junctions. Such single island circuits are fundamental building blocks for quantum electronic circuits based on the number-phase uncertainty of the Cooper pair condensate, and have been the object of growing interest due to their potential to realize new types of quantum limited measurements and solid state quantum bits. Essential for all these applications is the ability to inhibit the excitation of quasiparticles which give rise to dissipation (noise) and thereby decoherence. For the CPT this means that the charge parity of the island must be well-controlled, so that quasiparticles, or single unpaired electrons, are not transferred to or from the CPT island. Here we study the CPT in a tunable high frequency electrodynamic environment, where the dc current-voltage characteristic (IVC) of the CPT exhibits a Coulomb blockade of Cooper-pair tunneling. By tuning the impedance of the environment, we demonstrate how the parity of the island is controlled by the environment.

CPTs have been most extensively studied in a high frequency environment with low impedance, $Z_{\mathrm{env}} \ll R_Q \equiv h/4e^2 \simeq 6.45\ \mathrm{k}\Omega$, where the gate voltage modulates the critical current flowing through the device. At low temperature and in the absence of quasiparticle excitations, this modulation should be periodic in gate voltage with period $2e/C_g$, where C_g is the gate capacitance. $2e$-periodic modulation is a clear sign that charge transport through the device is due to Cooper pairs, which do not change the parity of the island. However, in many experiments this parity effect is spoiled by the transfer of quasiparticles to or from the island, resulting in an e-periodic gate modulation, or modified $2e$-periodic modulation, as the unpaired electron occupies the island. For applications like the coherent control of a quantum bit, these quasiparticles have to be avoided and several experimental studies have been carried out in order to understand and control this parity effect. Normal metal leads, or small normal metal "traps," contacting the superconducting source and drain close to the tunnel junctions, are thought to help bring long-lifetime out-of-equilibrium quasiparticles into thermal equilibrium and thereby enhance the parity effect.[1,2] However, in many experiments where no traps were used, a parity effect was demonstrated.[3–7] Aumentado *et al.*[5] showed that the lifetime of the unpaired quasiparticle on the island could be dramatically reduced by fabricating the island of the CPT with a larger superconducting energy gap than that of the source and drain electrodes.

Here we present an experimental study of the CPT in a high impedance environment, $Z_{\mathrm{env}} \gg R_Q$, where far less experimental work has been done due to the difficulty in constructing such an environment. In a high impedance environment, the IVC of the CPT shows not a supercurrent, but rather a Coulomb blockade of Cooper pair tunneling. The Coulomb blockade is modulated with the gate voltage and in the absence of quasiparticles this modulation is $2e$-periodic. Previously, the high impedance environment has been achieved with small on-chip resistors ($R \gg R_Q$) located close to the CPT, which have enabled the observation of a Coulomb blockade of Cooper pair tunneling with $2e$-periodic dependence on the gate charge.[8,9] More recently, one-dimensional superconducting quantum interference device (SQUID) arrays have been used to bias a CPT[10] which is the technique used in the present study. The great advantage of the SQUID arrays bias is that the impedance of the environment can be tuned *in situ*, without affecting the CPT. In this way the role of fluctuations due to the environment can be easily identified.

In this paper we study the IVC of the CPT as the environment impedance is changed over many orders of magnitude. Starting from a superconductinglike IVC at low impedance, a well-defined Coulomb blockade of Cooper pair tunneling with a back-bending IVC develops as the impedance of the environment is increased. This back-bending IVC is due to the coherent tunneling of single Cooper pairs and is a clear indication that $Z_{\mathrm{env}} \gg R_Q$. We show that the gate voltage dependence of the IVC changes from e-periodic to $2e$-periodic as the environment impedance is increased. The high impedance environment suppresses quasiparticle tun-

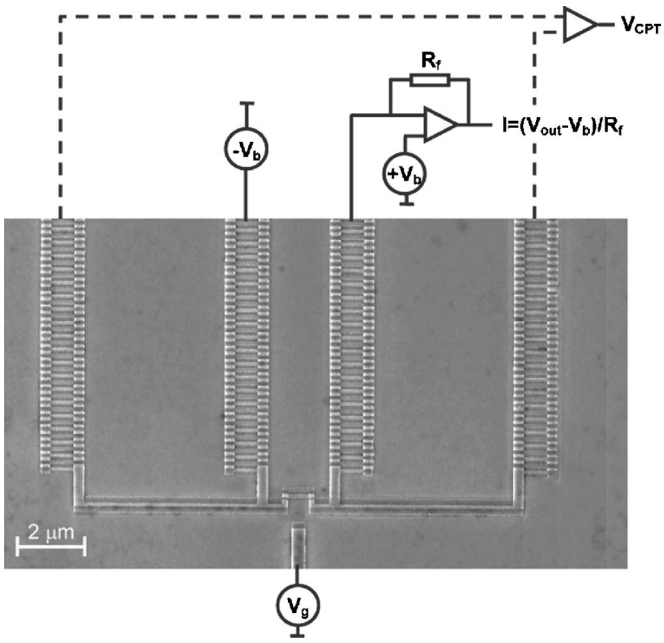

FIG. 1. SEM micrograph of a CPT (in the center) biased by four SQUID arrays. Two SQUID arrays are employed to apply a symmetric bias, while the other pair is used to measure the voltage across the CPT.

neling rates, thereby restoring the even parity of the island. These observations indicate new approaches for controlling out-of-equilibrium quasiparticles in superconducting quantum circuits.

II. FABRICATION AND MEASUREMENT

Figure 1 shows a scanning electron microscopy (SEM) micrograph of a sample containing 562 working junctions. The $Al/AlO_x/Al$ tunnel junctions are fabricated on a SiO_2/Si substrate using *e*-beam lithography and the standard shadow evaporation technique.[11] To provide an effective high impedance environment, the arrays have to be located close to the CPT, so as to avoid the shunting capacitance of the leads. Four arrays, each consisting of 70 SQUIDs in series, connect the CPT to the bias and measurement circuitry. The SQUIDs junctions are designed to have two identical critical currents $I_{C1}=I_{C2}$, in order to suppress the Josephson coupling in the array as low as possible. Because the loop inductance $L_{\text{loop}} \ll \hbar/2eI_{C1(2)}$, we can tune the critical current of the SQUID with an external magnetic flux, $I_C=(I_{C1}+I_{C2})\cos(\Phi_{\text{ext}}/\Phi_0)$ and thereby the SQUID inductance.

As will be detailed experimentally below, the arrays have large real impedance. Theoretically, little is known about the microscopic origin of this impedance. In Ref. 12, the finite resistance due to fluctuating dipoles was considered, whereas in Ref. 13 the role of dissipative quasiparticle processes has been suggested. Here we will infer some understanding from a simple model based on the distributed Josephson inductance of the SQUIDs. An infinite array can be modeled as a transmission line[14,11] with purely real characteristic impedance $Z_{\text{line}}=\sqrt{L_J/C_0}$. Here C_0 is the capacitance of each island in the array to ground and $L_J=\hbar/2eI_C\cos(\phi)$ is the SQUID inductance which becomes infinite as I_C is suppressed to zero with an external magnetic flux. This inductance is also nonlinear, as it depends on the phase ϕ (or current) across the SQUID, and therefore the impedance concept can only describe the electrodynamics of these arrays for low current, $I \ll I_C$. Nevertheless, the linear model of the array transmission line has a gap, or region of frequency where no propagating modes exist, resulting from the non-negligible junction capacitance $C \gg C_0$. A finite length array with unmatched termination impedance will have a set of discrete modes corresponding to standing wave Josephson plasmons (phase waves) in the array. The real part of the impedance will have a peak at each of the mode frequencies. For arrays such as the ones used in this study, the lowest frequency mode has $f \simeq 30$ GHz at zero magnetic field. Due to this high frequency scale, such modes have not yet been observed. However, we have shown that these arrays do provide an environment which induces a Coulomb blockade of Cooper-pair tunneling and Bloch oscillations in a single Josephson junction.[15,16] When the magnetic flux is tuned such that the characteristic impedance becomes large, $Z_{\text{line}} \geqslant R_Q$, the arrays undergo a quantum phase transition[17,18] and the measured zero bias resistance of the array increases several orders of magnitude ($50\ \text{k}\Omega < R_0 < 1\ \text{G}\Omega$). An important property of the arrays for experiments of the type here described is that they can be tuned in this transition region to a point where they provide a high enough impedance at high frequencies, while not having too large R_0. If R_0 becomes too large, the very small input offset current of the voltage amplifier will inhibit the measurement of the differential voltage across the CPT.

The chip with the arrays and CPT is bonded to a printed circuit board with connectors, which is mounted in a rf-tight box on a dilution refrigerator with a base temperature of 15 mK. The cryostat leads are twisted constatan pairs, which act as rather good microwave filters, attenuating 35 dB/GHz up to 2 GHz, above which a background transmission of −80 dB is measured with an open cryostat. Additional room temperature RC filters were used to suppress lower frequency noise when necessary. No microwave filters between the sample and twisted pairs were implemented in these measurements. However, in the high impedance case, the arrays themselves are good filters, protecting the CPT from electromagnetic fluctuations coming from the bias side of the arrays.

The IVC of the CPT is measured in a four point configuration with the CPT symmetrically biased through one pair of SQUID arrays, while the other pair is used to measure the voltage across the sample. The current is measured with a transimpedance amplifier (modified Stanford Research Systems 570) on one of the biasing leads. The voltage across the CPT is measured with a high input impedance differential voltage amplifier (Burr-Brown INA110). The bias voltages $\pm V_b$ are applied symmetrically with respect to ground in order to avoid a common mode drain-source voltage. In this way, a polarization charge can be induced on the island only by the voltage applied to the gate and not from a bias-induced common mode voltage acting across the stray capacitance of the CPT to ground.[11]

TABLE I. List of a few characteristic parameters of the measured CPT samples.

	r_N (kΩ)	R_N (kΩ)	C (fF)	E_J (μeV)	E_C (μeV)	E_J/E_C	V_t (μV)	V_{gap} (μV)
CPT 6	1.8	5.2	0.75	125	106	1.2	15	35
CPT 7	8.5	21	0.6	30	133	0.22	40	110
CPT 8	1.1	1.5	0.8	430	100	4.3	5	
CPT 9a	3.1	11.5	0.55	56	145	0.38	34	60
CPT 9b	3	8.2	0.55	80	145	0.55	26	45

The parameters of the measured samples are listed in Table I. The nominal area of each junction in a SQUID array is 0.03 μm^2 and the loop area is 0.18 μm^2. The normal state resistance r_N of a junction pair in the SQUID arrays is listed in Table I. Each CPT junction has a nominal area of 0.01 to 0.02 μm^2. The resistance R_N of one junction in the CPT is calculated from the slope of the IVC at large bias voltage, assuming that both junctions are identical. The Josephson energy is $E_J=(R_Q/R_N)(\Delta/2)$, where $\Delta\approx 200$ μeV is the superconducting energy gap of Al. The capacitance of one junction in the CPT is calculated from the junction area as measured from SEM pictures, using the specific capacitance 45 fF/μm^2. From the capacitance C, the charging energy of one junction in the CPT is calculated as $E_C=e^2/2C$. For all the measured samples $C_g\simeq 10$ aF$\ll C$, so that the total island capacitance is given by $C_\Sigma=C_1+C_2+C_g\approx 2C$. In Table I, V_t indicates the measured maximum threshold voltage for Cooper pairs, as determined from the IVC of the CPT when $Z_{\mathrm{env}}\gg R_Q$. V_{gap} refers to the maximum value of the measured Coulomb gap for single electrons, estimated from the offset of the normal state IVC, taken in high magnetic fields where superconductivity is completely suppressed.

III. CURRENT-VOLTAGE CHARACTERISTIC OF THE COOPER-PAIR TRANSISTOR IN A HIGH IMPEDANCE ENVIRONMENT

Most experimental and theoretical studies to date have considered the case of a CPT embedded in a low impedance environment, $Z_{\mathrm{env}}\ll R_Q$.[1–7,19] A few studies have been made for the case of a high impedance environment, $Z_{\mathrm{env}}\gg R_Q$.[8–10] Below we review the theoretical description of the CPT for the low impedance case, showing how it can be transformed to a description appropriate for the high impedance case. We then give a qualitative description of the IVC and Bloch oscillations for the latter case, comparing this with experimental results.

We consider the circuit depicted in Fig. 2, consisting of a symmetric CPT with $E_{J1}=E_{J2}=E_J$ and $C_1=C_2=C$. The charge induced by the gate on the island is $Q_g=C_gV_g$, where V_g is the voltage applied to the gate electrode. $Q_{1(2)}$ indicates the charge and $\phi_{1(2)}$ the phase difference across each junction. Let $\phi=\phi_1+\phi_2$ be the bias phase across the CPT and $\phi_g=(\phi_1-\phi_2)/2$ the phase of the island. The phases ϕ and ϕ_g are conjugate, respectively, to the charge transferred across the device $Q_\phi=(Q_1+Q_2)/2$ and the total island charge $Q=Q_1-Q_2+Q_g$ and obey the commutation relations $[Q_\phi,\phi]=[Q,\phi_g]=-2ie$.

For the moment we neglect the contribution of quasiparticles by assuming that the superconducting energy gap Δ is large compared to all relevant energy scales. The Hamiltonian of a CPT with $C_g\ll C$ biased by a current $I_b=V_b/Z_{\mathrm{env}}$ can be written as follows:

$$H=8E_C\left(\frac{Q_\phi}{2e}\right)^2+2E_C\left(\frac{Q+Q_g}{2e}\right)^2-2E_J\cos(\phi/2)\cos(\phi_g)-\frac{\hbar I_b\phi}{2e}. \quad (1)$$

The first term of the Hamiltonian corresponds to the charging energy associated with the total charge across the series combination of the two junctions of the CPT. The second term is the electrostatic energy associated with the island which sees the two junctions in parallel. The third term is the effective Josephson energy of the CPT, which, due to its dependence on ϕ_g, can be modulated by the gate voltage. The last term represents the coupling between the bias current I_b and the phase ϕ. For small I_b, the eigenstates of this Hamiltonian are approximately Bloch states,[21] $\psi_{\nu,q,q_g}(\phi,\phi_g)$. Here ν is the index labeling the Bloch bands which we will discuss below. In the presence of I_b, the perfect periodicity with respect to ϕ is broken, therefore the corresponding quasicharge q is a continuous variable. The periodicity with respect to ϕ_g is not affected by I_b, the relevant quasicharge q_g thus takes values $2ne$ with integer n only. The shift of Q by Q_g in Hamiltonian (1) shifts the quasicharge to $q_g=Q_g+2ne$.[23] Therefore we will base our analysis of the Bloch bands of the CPT presented below on Bloch states $\psi_{\nu,q,Q_g}(\phi,\phi_g)=e^{i\phi q/(2e)}e^{i\phi_gQ_g/(2e)}u_\nu(\phi,\phi_g)$, where u_ν is a periodic function satisfying $u_\nu(\phi+4\pi,\phi_g+2\pi)=u_\nu(\phi,\phi_g)$.

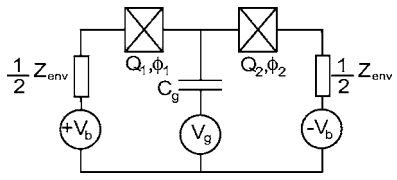

FIG. 2. Schematic of a Cooper pair transistor. The environment is represented by the impedance Z_{env}. When $Z_{\mathrm{env}}\ll R_Q$ ($Z_{\mathrm{env}}\gg R_Q$) the CPT is embedded in a low (high) impedance environment. $Q_{1(2)}$ indicates the charge and $\phi_{1(2)}$ the phase difference across each junction.

In a low impedance environment, $Z_{\mathrm{env}} \ll R_Q$, quantum fluctuations of the phase are suppressed and the bias phase ϕ behaves as a classical variable. Due to the low impedance, Cooper pair tunneling at zero bias voltage dominates the IVC of the CPT which shows the typical superconducting behavior characterized by a supercurrent branch at vanishing voltages. When $E_J \ll E_C$, charging effects are observable and result in a $2e$-periodic modulation of the critical current with the gate charge. Thus when $Z_{\mathrm{env}} \ll R_Q$, the CPT behaves as a single Josephson junction with a gate charge dependent critical current.[1,2]

Let us turn to the case of a high impedance environment, $Z_{\mathrm{env}} \gg R_Q$, where quantum fluctuations of the phase are strong and the conjugate charge now becomes a classical variable. For this case, a quantitative theory of the single Josephson junction in terms of Bloch energy bands has been developed.[20,21] Here the Josephson coupling (periodic potential) naturally gives rise to a description of the state of the junction, in terms of quasicharge, which has a direct relation to the current I flowing through the junction $q = \int I dt$. The circuit dynamics are then described in terms of quasicharge by the Langevin equation

$$\frac{dq}{dt} = (I_b + \delta I) - \frac{V(q)}{R}, \tag{2}$$

where $V(q)$ is the voltage across the junction and δI indicates a random noise component of the bias current, induced by the real impedance of the environment $R = \mathrm{Re}[Z_{\mathrm{env}}] \gg R_Q$ at finite temperature. The voltage $V(q)$ is given by the derivative of the lowest Bloch energy band, $V(q) = dE_0/dq$. The IVC of the junction can be calculated analytically from the Langevin equation[20–22] and shows a voltage peak near zero current corresponding to the Coulomb blockade of Cooper pair tunneling and a back-bending region at finite currents. This region of negative differential resistance is the indication of the Bloch oscillations which occur with frequency $f_B = \langle I \rangle / 2e$.

The natural extension of the Bloch band picture from a single Josephson junction to a CPT leads to a description of the quasicharge dynamics in two-dimensional Bloch energy bands. This description becomes clear if we first rewrite the Hamiltonian (1) for $I_b = 0$ and $Q_g = 0$ in terms of the variables $Q_{1(2)}$ and $\phi_{1(2)}$, such that

$$H = 4E_C \left(\frac{Q_1}{2e} \right)^2 + 4E_C \left(\frac{Q_2}{2e} \right)^2 - E_J \cos(\phi_1) - E_J \cos(\phi_2). \tag{3}$$

This Hamiltonian is that of two, independent single Josephson junctions $H_{1(2)} = 4E_C (Q_{1(2)}/2e)^2 - E_J \cos(\phi_{1(2)})$. In this case the lowest energy band $\nu = 0$ of the CPT is given by the sum of the lowest energy band of the two single junctions, that is $E_0(q_1, q_2) = E_0(q_1) + E_0(q_2)$, see Fig. 3, where we plot the lowest band as a function of the quasicharges q_1 and q_2, which describe the dynamics of the two junctions of the CPT.

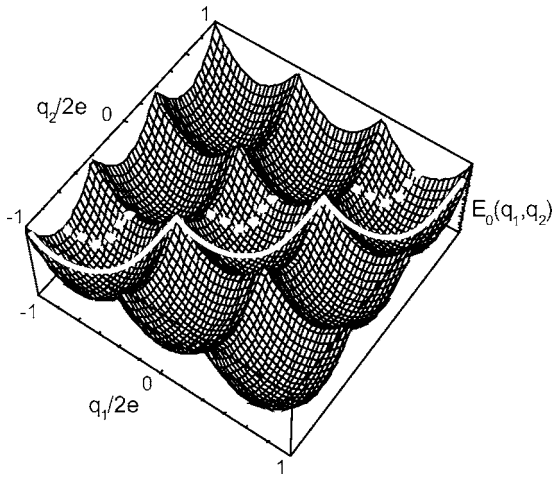

FIG. 3. Lowest energy Bloch band for a CPT with $E_J/E_C \ll 1$. For fixed gate charges, the quasicharges q_1 and q_2 follow a diagonal trajectory. The solid and dotted lines indicate, respectively, the quasicharges trajectories for $Q_g = 0$ and $Q_g = e$.

We now relate the quasicharges q_1 and q_2 to the quasicharges q and Q_g introduced above in order to understand the effect of nonzero bias current and gate-charge. We rewrite the phase factors of the Bloch states in terms of the variables ϕ_1 and ϕ_2 and find $e^{i\phi q/(2e)} e^{i\phi_g Q_g/(2e)} = e^{i\phi_1 (q + Q_g/2)/(2e)} e^{i\phi_2 (q - Q_g/2)/(2e)}$. We thus identify the relation between the two quasicharges q_1 and q_2 of each junction on the one hand and the gate-induced charge $q_1 - q_2 = Q_g + 2ne$ and the total quasicharge $q = (q_1 + q_2)/2$ on the other hand. As we discussed above, in the presence of small bias current $I_b \neq 0$, we expect the Bloch states to still give a good description of the CPT. Since it breaks the perfect periodicity of the Hamiltonian with respect to the variable $\phi_1 + \phi_2$, total quasicharge $q = (q_1 + q_2)/2$ should be treated as a continuous variable. The Hamiltonian is perfectly periodic with respect to the phase difference $\phi_1 - \phi_2$, reflecting charge quantization on the island and leading to discreteness of the quasicharge difference $q_1 - q_2 = Q_g + 2ne$. For a fixed gate charge, this constrains the quasicharge to a diagonal trajectory in the two-dimensional Bloch band (Fig. 3). A change in the gate voltage induces a shift in the trajectory of the two quasicharges, as shown in Fig. 3. This constraint makes possible an analogy to the single junction case, where the voltage across the CPT can then be expressed via the derivative of the lowest energy band along the diagonal direction $V(q) = dE_0(q_1, q_2)/dq$. However, the maximum Coulomb blockade voltage, or critical voltage $V_C = \max[dE_0(q_1, q_2)/dq]$, is now a $2e$-periodic function of the gate charge. The dependence of the critical voltage on the gate charge is determined by the slope of the energy band according to the Bloch band theory.[9] The critical voltage is maximum when $Q_g = 0$, where the slope of the lowest energy band is maximized (solid line in Fig. 3), while the minimum critical voltage is obtained for $Q_g = e$ (dotted line in Fig. 3).

Thus when $Z_{\mathrm{env}} \gg R_Q$ the CPT behaves as a single Josephson junction with a gate charge dependent critical voltage. In the case $Q_g = 0$, the energy-charge relation of the CPT is identical to that of a single Josephson junction and the volt-

age $V(q)$ across the CPT has a $2e$-periodic dependence on the quasicharge. From the band diagram one can see that as the gate charge is shifted, the dependence of the voltage on the quasicharge is modified. When $Q_g=e$, the energy-charge relation is e-periodic. Physically, this shift in gate charge brings the Bloch oscillations in each junction out of phase, resulting in an oscillation of the voltage across the CPT with frequency $f=e/\langle I\rangle$.[9] For $E_J>E_C$, the lowest Bloch band becomes more sinusoidal along the quasicharge axes and the diagonal trajectory at $Q_g=e$ becomes flat for a symmetric CPT. In this case the Coulomb blockade for Cooper pairs can be modulated to zero and the out-of-phase Bloch oscillations cancel one another.

The IVC of a CPT in the high impedance environment shows the same features as that for a single Josephson junction and can be calculated from the Langevin equation for the quasicharge (2). We can picture how the Bloch oscillations occur in the CPT, or single Josephson junction with tunable critical voltage, by simply considering a nonlinear capacitor biased by a voltage source V_b through a resistor $R \gg R_Q$. In Fig. 4 the generic shape of the IVC is shown, with the time evolution of the junction voltage sketched for four different operating points of the circuit. We consider the case $E_J<E_C$, where the nonlinear capacitor has a periodic, sawtooth form of the voltage-charge relation, given by the derivative of the lowest energy band along a diagonal trajectory with a maximum critical voltage. When the bias voltage is below the critical voltage, $V_b<V_C$ (operating point a), the Langevin equation (2) will have a stationary solution with $I=dq/dt=0$ and the nonlinear capacitor will simply charge up to the value V_b with no voltage oscillation. As the bias is increased so that $V_b>V_C$, time dependent solutions to the Langevin equation are possible, which describe overdamped, forced Bloch oscillations in the junction. These oscillations result in a periodic charging and discharging of the nonlinear capacitor, which lead to a time average voltage $\langle V\rangle<V_C$ (operating point b). As the bias voltage is further increased, the Bloch oscillations increase in frequency as higher current is forced through the junction. With faster Bloch oscillations, the finite charging time due to the bias resistor becomes negligible and the voltage oscillations become more symmetric around zero, with $\langle V\rangle \to 0$ (operating point c). Increasing the bias voltage further would cause back-bending of the IVC to dissipationless transport, or dc current with zero average voltage. However, with higher frequency Bloch oscillations, Zener tunneling to higher energy bands takes place, resulting in a temporary build-up of the junction voltage to a level close to the superconducting energy gap.[23] In this case, quasiparticle tunneling can no longer be neglected and Josephson quasiparticle tunneling cycles, which are dissipative processes, can occur. As the Zener tunneling probability increases with the bias current, the time average voltage across the junction increases (operating point d). The magnitude of the Zener current depends on the energy gap between the lowest and first Bloch energy band, which in turn depends on the ratio E_J/E_C.[23,24]

We find qualitative agreement with this theoretical picture in our experimental IVCs of CPTs biased by SQUID arrays. Figure 5(a) shows the IVC of two biasing SQUID arrays of

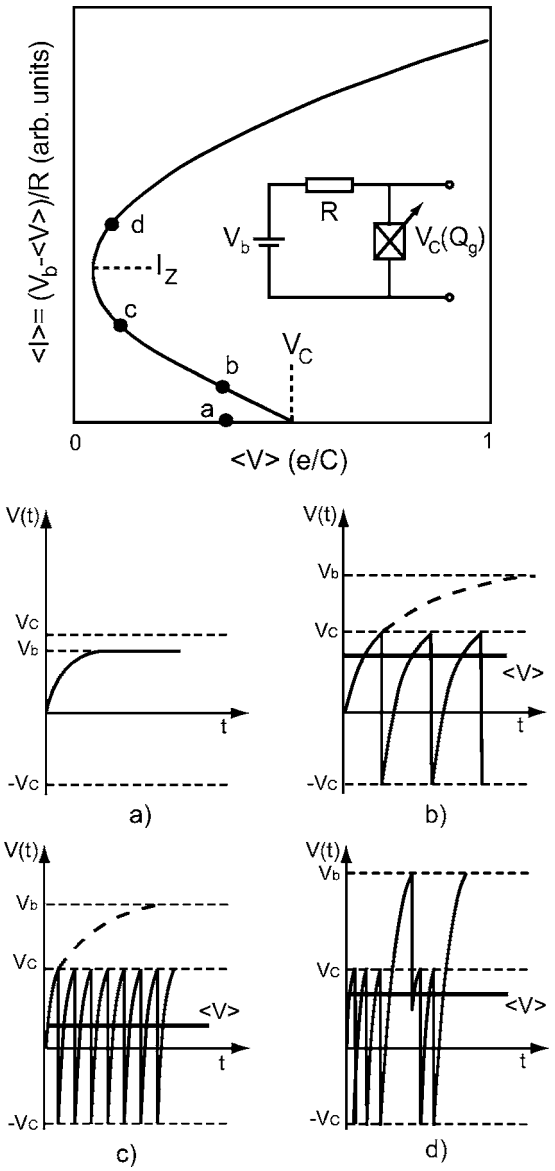

FIG. 4. A pictorial description of the Bloch oscillations and back-bending IVC of a CPT, or single Josephson junction with tunable critical voltage V_C, current biased by a high impedance resistor. I_Z indicates the Zener current. The time dependence of the voltage across the junction is shown for four different operating points in the IVC. The shape of the Bloch oscillations refers to the case of a junction with $E_J \ll E_C$.

sample CPT 9a measured in series at three values of the magnetic field, between zero and $\Phi_0/2$. Here we see that the arrays change their zero bias resistance R_0 over several orders of magnitude as the Josephson coupling of the SQUIDs is suppressed. In Fig. 5(b) the corresponding IVCs of the CPT are plotted for the same magnetic fields. At low R_0 of the arrays, the IVC of the CPT shows a superconductinglike feature that disappears as the Coulomb blockade region becomes progressively more defined for increasing values of R_0. When $R_0 \approx 20$ MΩ, the Coulomb blockade for Cooper pairs is fully developed and is followed by a region of negative differential resistance. This back-bending IVC is the hallmark feature of a Coulomb blockade of Cooper pair tun-

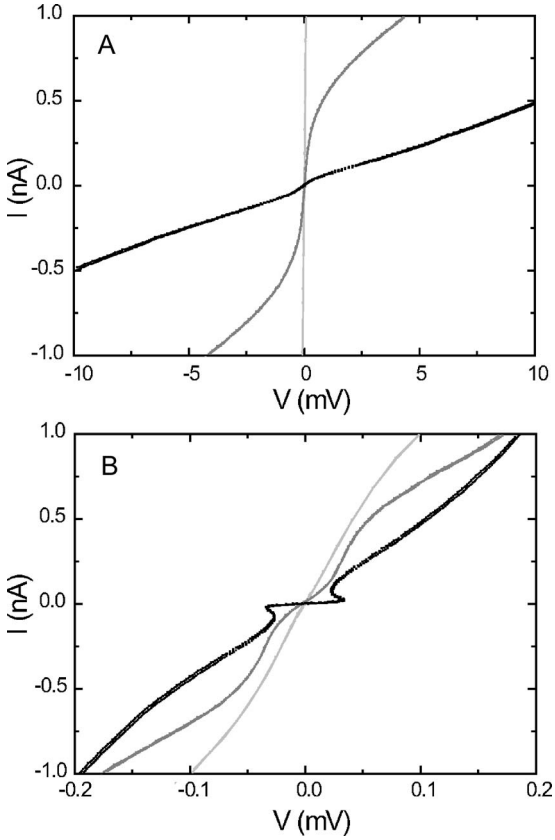

FIG. 5. (a) IVC of the two biasing SQUID arrays of sample CPT 9a for different magnetic fields. The measured values for R_0 are light-gray curve $R_0 \approx 50$ kΩ, dark-gray curve $R_0 \approx 500$ kΩ, and black curve $R_0 \approx 20$ MΩ. (b) Corresponding IVCs of CPT 9a.

neling and clear evidence that a high impedance of the environment has been achieved. Figure 6 shows the IVC of three different CPT samples with different values of E_J/E_C. In each case the SQUID arrays are tuned to approximately the same value of R_0 where the back-bending IVC is well-defined. Figure 6 clearly demonstrates the agreement with

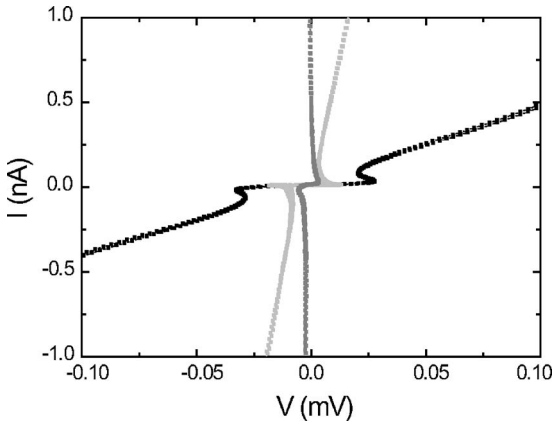

FIG. 6. The IVC for three different CPTs having approximately the same value of the zero bias resistance of the SQUID arrays ($R_0 \approx 20$ MΩ). Black curve: CPT 9a, $E_J/E_C=0.38$, light-gray curve: CPT 6, $E_J/E_C=1.2$, and dark-gray curve: CPT 8, $E_J/E_C=4.3$.

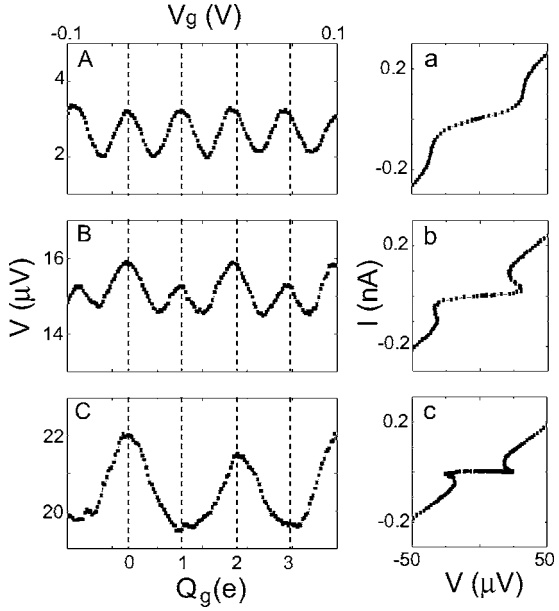

FIG. 7. (A,B,C) Gate-induced voltage modulation of sample CPT 9a for increasing values of the zero bias resistance of the biasing SQUID arrays. The bias current is fixed at $I_b=5$ pA. (a,b,c): IVC of the CPT for the same values of R_0. (A,a): $R_0 \approx 1$ MΩ, (B,b): $R_0 \approx 5$ MΩ, and (C,c): $R_0 \approx 40$ MΩ.

the theory described above. With increasing E_J/E_C, the critical voltage decreases, as the lowest Bloch band develops more shallow minima. We also see that the Zener current becomes larger with increasing E_J/E_C, as the gap to higher energy bands becomes larger. A full quantitative comparison of the back-bending IVC with theory is possible in the case $E_J \gg E_C$.[16]

IV. GATE VOLTAGE MODULATION AND IMPEDANCE DEPENDENT PARITY EFFECT

As discussed in the previous section, the two-dimensional Bloch band picture describing transport in the CPT in terms of the quasicharge leads to a $2e$-periodic modulation of the IVC with gate voltage. This picture only considers Cooper-pair tunneling, completely neglecting quasiparticle or single electron tunneling. If the single electron tunneling rates are large enough they can disrupt this picture, causing e-periodic modulation of the IVC. In our experiments we find that the impedance of the environment can be used to suppress these quasiparticle tunneling rates low enough for stable $2e$-periodic behavior to be observed. Figure 7 shows how the periodic modulation of the threshold voltage with gate at a constant current $I_b=5$ pA evolves from $2e$-periodic to e-periodic as the impedance of the environment is tuned. At high impedance, where the Coulomb blockade is well-developed, we find $2e$-periodic behavior as expected from the two-dimensional Bloch band picture [Fig. 7(c)]. As the impedance of the environment is reduced, the effect of "quasiparticle poisoning" is seen as a small peak in the threshold voltage at gate charges $Q_g=(2n+1)e$ [Fig. 7(b)], which grows until an e-periodic behavior is observed [Fig. 7(a)]. A

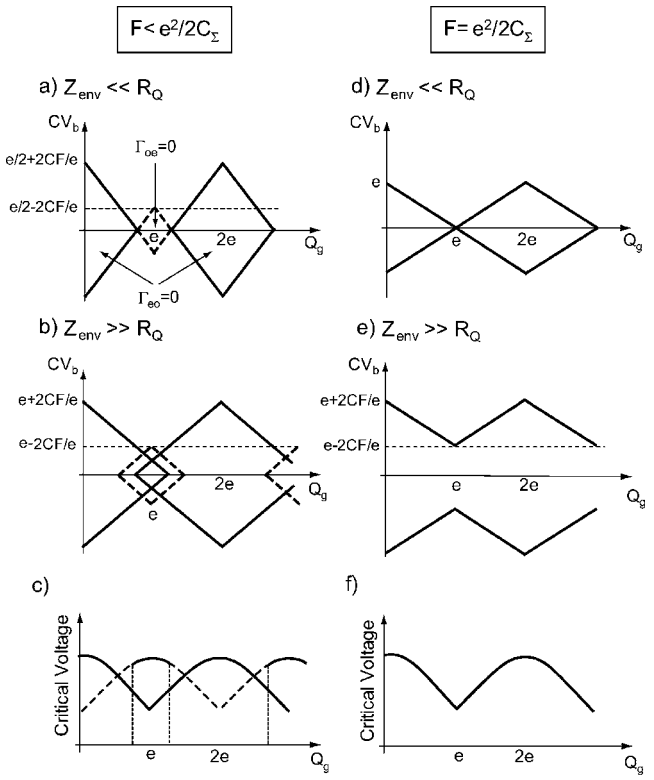

FIG. 8. (a)–(d) Stability diagrams for the cases $F<E_{C_\Sigma}$ with $Z_{\mathrm{env}}\ll R_Q$ and $Z_{\mathrm{env}}\gg R_Q$ [(a) and (b)], $F=E_{C_\Sigma}$ with $Z_{\mathrm{env}}\ll R_Q$ and $Z_{\mathrm{env}}\gg R_Q$ [(d) and (e)]. (c) e-periodic gate voltage dependence of the critical voltage at finite bias voltage $(V_b<e/C-2F/e)$ corresponding to the stability diagrams of (a),(b), and (d). (f) $2e$-periodic gate voltage dependence of the critical voltage at finite bias voltage $(V_b<e/C-2F/e)$ corresponding to the case (e).

similar crossover from $2e$ to e-periodic behavior as the environment impedance is tuned has been observed by Watanabe[10] and Kuo *et al.*[25]

Below we propose a simple model to explain this crossover as a function of environment impedance. In this simple model we include the presence of thermally excited quasiparticles on top of the condensate of Cooper pairs. Since, apart from the gate modulation, the detailed shape of the measured IVC can be completely explained by Cooper pair dynamics,[16] the only effect of the presence of these quasiparticles will be to change the parity of the island. In particular this means we ignore more complicated processes involving Cooper pairs and quasiparticles like, for example, Josephson quasiparticle cycle or $3e$ tunneling processes.[26–28]

To understand how quasiparticles affect the critical voltage of a symmetric CPT in a tunable environment it is instructive to determine the regions in the bias voltage–gate voltage plane where it is energetically favorable for a single quasiparticle to tunnel on or off the island, thereby changing the island parity. As we will see, the shape of the corresponding stability diagrams depends on the impedance of the environment as well as on the ratio of the two characteristic energies for adding or removing a single quasiparticle to or from the island. These energies are the charging energy of the island $E_{C_\Sigma}=e^2/2C_\Sigma$ and the free energy difference $F=\Delta-k_BT\ln(N_{\mathrm{eff}})$ that lifts the odd parity from the even parity states.[1,4,19] Here, the entropy term involves $N_{\mathrm{eff}}=N(0)V\sqrt{2\pi\Delta T}$, the number of quasiparticle states available within temperature T just above the gap ($N(0)$ is the normal-state density of states at the Fermi level and V the volume of the island). At zero temperature, $N_{\mathrm{eff}}=0$ and this energy difference is the superconducting energy gap Δ which is paid for having one unpaired electron on the island. The free energy difference F vanishes at a temperature $k_BT^*=\Delta/\ln(N_{\mathrm{eff}})$.

Let us first consider the situation of a free energy difference smaller than the island charging energy, $F<E_{C_\Sigma}$. In Fig. 8(a) we plot the corresponding stability diagram for the case of a low impedance environment where charge redistributes immediately. When considering energy differences the entire double junction circuit has to be taken into account, including the work done by the voltage source. This corresponds to the so-called global rule description.[29] The stability diagram contains lines which separate regions in the bias voltage–gate voltage plane with stable parity from regions where it is energetically favorable for a single quasiparticle to tunnel on or off the island, thereby changing the parity. Within the dotted rhombi the transition rate Γ_{oe} from odd to even parity is zero, while within the solid rhombi the rate from even to odd parity Γ_{eo} vanishes. Outside the rhombi, a parity change corresponds to a decrease in energy and the transition rates Γ_{oe} and Γ_{eo} are nonzero at $T=0$. We conclude that the odd parity states are stable near the gate charges $Q_g=(2n+1)e$ [Fig. 8(a)]. At these gate charges the system will be "poisoned" by the excess quasiparticle which sits on the island in the lower energy state. When in the odd parity state, the effective island charge is shifted by e and we thus expect the gate voltage dependence of the critical voltage of the CPT to be shifted correspondingly [from the solid to the dashed line in Fig. 8(c)]. In particular, as gate voltage is changed, the critical voltage should have two maxima per $2e$-period [near gate charges $Q_g=(2n+1)e$ and $Q_g=2ne$]. This is in qualitative agreement with the low impedance data of Figs. 7(A) and 7(B).

In a high impedance environment, charge redistribution is slow and when considering energy differences one only needs to consider the junction through which the quasiparticle is tunneling. This corresponds to the local rule description,[29] which should be applied to establish the stability diagrams. As a result, the size of the rhombi doubles and various stability regions start to overlap. Overlap means that there are bistable regions where either parity is stable, depending on the history of the system. However, as can be seen in Fig. 8(b), for $F<E_{C_\Sigma}$ odd stability regions (dashed rhombi) still exist near gate charges $Q_g=(2n+1)e$ and we expect the critical voltage to show two maxima per $2e$ period. This observation is in contradiction with the experimental high impedance data shown in Fig. 7(C), where only one critical voltage maximum per $2e$ period is observed, near gate charges $Q_g=2ne$.

We therefore consider the stability diagram for the case $F\sim E_{C_\Sigma}$, first in a low impedance environment, as shown in Fig. 8(d). Compared to the case $F<E_{C_\Sigma}$ [Fig. 8(a)], the odd stability regions now disappear, giving rise to regions near the gate charges $Q_g=(2n+1)e$ where both rates $\Gamma_{\mathrm{oe}},\Gamma_{\mathrm{eo}}\neq 0$

and parity will fluctuate at small bias voltage. However, in a high impedance environment for $F \sim E_{C_\Sigma}$, as shown in Fig. 8(e), we observe that the odd stability regions completely disappear, giving way to overlapping regions of even stability only, as long as the applied bias voltage satisfies the inequality $V_b < e/C - 2F/e$. This is markedly different from the low impedance case, where regions of fluctuating parity exist at any finite bias. We thus conclude that the critical voltage is $2e$-periodic as a function of gate voltage [Fig. 8(f)] for high impedance and $F \sim E_{C_\Sigma}$, in agreement with the experimental findings of Fig. 7(C).

This stability analysis shows that quasiparticle poisoning can occur near the gate charges $Q_g = (2n+1)e$ if conditions are not favorable. The measured long-time average CPT voltage near these gate charges will depend on the relative weight of the odd and even states, which are fluctuating on a much more rapid time scale determined by the rates Γ_{oe}, Γ_{eo}. The value of these rates cannot be inferred from the stability analysis alone.[30] For $\Gamma_{oe} \gg \Gamma_{eo}$ the effective island charge will most often be even, hence the measured voltage of the CPT will have a minimum near $Q_g = (2n+1)e$ [see Fig. 8(f)]. The effects of poisoning will not be noticed on the long time scale of the experiment and one observes a stable $2e$-periodic modulation of transport. In the opposite case $\Gamma_{oe} \ll \Gamma_{eo}$, near $Q_g = (2n+1)e$ the decay of the odd state is much slower than that of the even state. The effective island charge will be predominantly odd and the measured average voltage, instead of taking a minimum value, will reach a local maximum, that eventually may become equal to the maxima found at $Q_g = 2ne$ [see Fig. 8(c)]. The measurements for low impedance presented in Fig. 7(A) show e-periodicity of the critical voltage with gate voltage, we conclude that the ratio $\Gamma_{oe} \ll \Gamma_{eo}$. This is in agreement with several other experiments on CPTs with $F \sim E_{C_\Sigma}$ in low impedance environments.[5,6,31–33] We also note that the observed e-periodicity excludes that F is large compared to E_{C_Σ}. If $F > E_{C_\Sigma}$, we would have found overlapping regions of stable even parity near $Q_g = (2n+1)e$, rather than regions of fluctuating parity and the resulting dependence of critical voltage on gate voltage would have been $2e$-periodic in the low impedance case.

We finally comment on the effect of finite temperature. The energy difference F depends on temperature T. For the islands used in this experiment, the characteristic crossover temperature T^* where $F \to 0$ can be estimated to be approximately 250 mK. The temperature T appearing in the expression for F does not necessarily correspond to the cryostat temperature, and could be an effective temperature, describing the fluctuations in the environment. Previous analysis of single junctions IVCs biased by similar arrays[16] showed an effective noise temperature of approximately 150 mK. At this temperature the ratio F/E_{C_Σ} is in the range 0.5–0.7 for the measured samples. Considering the uncertainties in estimating F and the junctions capacitance, we conclude that the assumption made above, $F \sim E_{C_\Sigma}$, is reasonable. A second effect of thermal fluctuations is that they mix states of different parity whose energy difference is $\lesssim k_B T$. On the level of the stability diagrams this means that the lines separating stability regions of different parity smear into strips whose width is $\sim C k_B T/e$. For the low impedance case this has drastic effects, even at low bias, because it leads to broadening of the parity fluctuation regions near $Q_g = (2n+1)e$ thereby enhancing the e-periodic gate modulation. For high impedance the even parity stability region has a gap with respect to the bias voltage, therefore thermal fluctuations do not effect the $2e$-periodicity as long as $k_B T < e^2/C - 2F \sim e^2/2C$. The fact that parity stability is robust against fluctuations for small bias voltage in a high impedance environment is directly connected with the inelastic nature of tunneling in this limit. This inelasticity is at the origin of the bias voltage gap and leads to an exponential suppression of quasiparticle tunneling at low bias voltage. This effect is absent for a low impedance environment where tunneling is elastic.

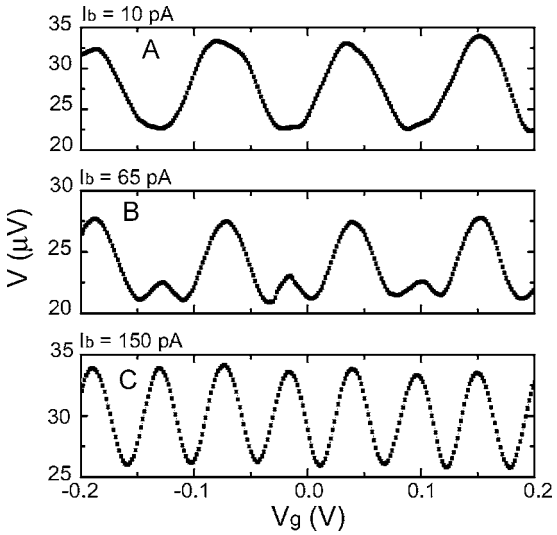

FIG. 9. Gate voltage modulation for sample CPT 9a at various bias current. The zero bias resistance of the biasing SQUID arrays is $R_0 \approx 20$ MΩ. The IVC of the CPT for this magnetic field is shown in Fig. 5.

The condition for stable $2e$-periodic behavior is not preserved at all bias currents in the high impedance environment. Figure 9 shows the gate voltage modulation for high impedance ($R_0 \approx 20$ MΩ) of the CPT voltage for three different values of the bias current. From low current levels up to the back-bending region of the IVC, the voltage modulation is stable $2e$-periodic [Fig. 9(a)]. As the current is increased toward the Zener current, which for this sample is measured at $I_Z \approx 75$ pA, the rate of single electron transitions increases, as explained in the previous section. Zener tunneling causes an increase in the rate Γ_{eo} near $Q_g = (2n+1)e$ and the effect of poisoning can be observed [Fig. 9(b)]. At even higher currents, the quasiparticle tunneling rate is so large that only e-periodic modulation can be seen [Fig. 9(c)].

V. CONCLUSIONS

The effect of the electrodynamic environment on single charge tunneling in the Cooper pair transistor (CPT) has been studied experimentally by biasing and measuring the CPT through one-dimensional SQUID arrays. The impedance of these arrays can be tuned with an external magnetic

field without changing the parameters of the CPT, which allows one to clearly discern the effect of the environment on tunneling. As the impedance of the arrays is increased, the CPT develops a Coulomb blockade of Cooper pair tunneling with a well-defined back-bending IVC, indicative of the coherent transfer of single Cooper pairs. The general shape of the measured IVC is that predicted by a theory based on quasicharge dynamics. We find that the observed threshold voltage depends on the ratio between the Josephson energy and the charging energy in a way that is in qualitative agreement with the Bloch band theory for the CPT. As the impedance of the environment is increased, we observe a transition from e-periodic to $2e$-periodic modulation of the IVC, demonstrating that the high impedance environment restores the parity effect in the CPT. Enhanced parity effect, or reduced quasiparticle poisoning, is explained by the inelastic nature of single-charge tunneling in a high impedance environment, where a charging energy gap makes odd parity states unstable near gate charges $Q_g=(2n+1)e$.

ACKNOWLEDGMENTS

This work was partially supported by the Swedish VR, SSF NanoDev program and the EU project SQUBIT. Samples were made in the KTH Nanofabrication laboratory, provided by the K. A. Wallenberg foundation. F.W.J.H. acknowledges support from the Institut Universitaire de France.

[1] P. Joyez, P. Lafarge, A. Filipe, D. Esteve, and M. H. Devoret, Phys. Rev. Lett. **72**, 2458 (1994).
[2] P. Ågren, J. Walter, and D. Haviland, Phys. Rev. B **66**, 014510 (2002).
[3] L. J. Geerligs, V. F. Anderegg, J. Romijn, and J. E. Mooij, Phys. Rev. Lett. **65**, 377 (1990).
[4] M. T. Tuominen, J. M. Hergenrother, T. S. Tighe, and M. Tinkham, Phys. Rev. Lett. **69**, 1997 (1992).
[5] J. Aumentado, M. W. Keller, J. M. Martinis, and M. H. Devoret, Phys. Rev. Lett. **92**, 066802 (2004).
[6] J. Männik and J. E. Lukens, Phys. Rev. Lett. **92**, 057004 (2004).
[7] A. Amar, D. Song, C. J. Lobb, and F. C. Wellstood, Phys. Rev. Lett. **72**, 3234 (1994).
[8] D. B. Haviland, Y. Pashkin, and L. S. Kuzmin, Physica B **203**, 347 (1994).
[9] A. B. Zorin, S. V. Lotkhov, Y. A. Pashkin, H. Zangerle, V. A. Krupenin, T. Weimann, H. Scherer, and J. Niemeyer, J. Supercond. **12**, 747 (1999).
[10] M. Watanabe, Phys. Rev. B **69**, 094509 (2004).
[11] S. Corlevi, Ph.D. thesis, Royal Institue of Technology, Stockholm, 2006.
[12] K. B. Efetov, Zh. Eksp. Teor. Fiz. **78**, 2017 (1980) [Sov. Phys. JETP **51**, 1015 (1980)].
[13] R. Lutchyn, L. Glazman, and A. Larkin, Phys. Rev. B **72**, 014517 (2005).
[14] D. B. Haviland, K. Andersson, and P. Ågren, J. Low Temp. Phys. **118**, 733 (2000).
[15] M. Watanabe and D. B. Haviland, Phys. Rev. Lett. **86**, 5120 (2001).
[16] S. Corlevi, W. Guichard, F. W. J. Hekking, and D. B. Haviland, Phys. Rev. Lett. **97**, 096802 (2006).
[17] E. Chow, P. Delsing, and D. B. Haviland, Phys. Rev. Lett. **81**, 204 (1998).
[18] W. Kuo and C. D. Chen, Phys. Rev. Lett. **87**, 186804 (2001).
[19] K. A. Matveev, M. Gisselfält, L. I. Glazman, M. Jonson, and R. I. Shekhter, Phys. Rev. Lett. **70**, 2940 (1993).
[20] D. V. Averin, A. B. Zorin, and K. K. Likharev, Zh. Eksp. Teor. Fiz. **88**, 692 (1985) [Sov. Phys. JETP **61**, 407 (1985)].
[21] K. K. Likharev and A. B. Zorin, J. Low Temp. Phys. **59**, 347 (1985).
[22] I. S. Beloborodov, F. W. Hekking, and F. Pistolesi, *New Directions in Mesoscopic Physics (Towards Nanoscience)* (Kluwer Academic Publisher, Dordrecht, 2002), p. 339.
[23] G. Schön and A. D. Zaikin, Phys. Rep. **198**, 237 (1990).
[24] D. V. Averin and K. K. Likharev, in *Mesoscopic Phenomena in Solids*, edited by B. L. Altshuler, P. A. Lee, and R. A. Webb, Vol. 30 of *Modern Problems in Condensed Matter Sciences* (North-Holland, Amsterdam, 1991), Chap. 6, pp. 173–272.
[25] W. Kuo and C. D. Chen, abstract presented at MS+S 2006, Atsugi, Japan.
[26] P. Hadley, E. Delvigne, E. H. Visscher, S. Lähteenmäki, and J. E. Mooij, Phys. Rev. B **58**, 15 317 (1998).
[27] A. Maassen v. d. Brink, A. A. Odintsov, P. A. Bobbert, G. Schön, and J. E. Mooij, Z. Phys. B: Condens. Matter **85**, 459 (1991).
[28] J. Siewert and G. Schön, Phys. Rev. B **54**, 7421 (1996).
[29] G.-L. Ingold and Y. V. Nazarov, in *Single Charge Tunneling. Coulomb Blockade Phenomena in Nanostructures*, edited by H. Grabert and M. H. Devoret, Vol. 294 of *NATO ASI Series* (Plenum Press, New York, 1992), Chap. 2, pp. 21–107.
[30] G. Schön, J. Siewert, and A. D. Zaikin, Physica B **203**, 340 (1994).
[31] P. Ågren, Ph.D. thesis, Royal Institue of Technology, Stockholm, 2002.
[32] C. van der Wal and J. E. Mooij, J. Supercond. **12**, 807 (1999).
[33] T. M. Eiles and J. M. Martinis, Phys. Rev. B **50**, 627 (1994).